

Empirical Regularized Optimal Transport: Statistical Theory and Applications

Marcel Klatt * Carla Taveling * Axel Munk *[†]

April 21, 2022

Abstract

We derive limit distributions for certain empirical regularized optimal transport distances between probability distributions supported on a finite metric space and show consistency of the (naive) bootstrap. In particular, we prove that the empirical regularized transport plan itself asymptotically follows a Gaussian law. The theory includes the Boltzmann-Shannon entropy regularization and hence a limit law for the widely applied Sinkhorn divergence.

Our approach is based on an application of the implicit function theorem to necessary and sufficient optimality conditions for the regularized transport problem. The asymptotic results are investigated in Monte Carlo simulations. We further discuss computational and statistical applications, e.g. confidence bands for colocalization analysis of protein interaction networks based on regularized optimal transport.

Keywords Regularized optimal transport, Sinkhorn divergence, limit law, sensitivity analysis, bootstrap, colocalization

MSC 2010 subject classification Primary: 62E20, 62G20, 65C60
Secondary: 90C25, 90C31, 90C59

1 Introduction

The theory of optimal transport (OT) has a long history in physics, mathematics, economics and related areas, see e.g. [Monge \(1781\)](#), [Kantorovich and Rubinstein \(1958\)](#), [Rachev and Rüschendorf \(1998\)](#), [Villani \(2008\)](#) and

*Institute for Mathematical Stochastics, University of Göttingen, Goldschmidtstraße 7, 37077 Göttingen

[†]Max Planck Institute for Biophysical Chemistry, Am Faßberg 11, 37077 Göttingen

Galichon (2016). Recently, also OT based *data analysis* has become popular in many areas of application, among others, in computer science (Schmitz et al., 2018; Balikas et al., 2018), mathematical imaging (Rubner et al., 2000; Ferradans et al., 2014; Adler et al., 2017) and machine learning (Arjovsky et al., 2017; Lu et al., 2017).

In this paper, we are concerned with certain statistical aspects of regularized optimal transport on a finite number of support points, e.g. representing spatial locations. To this end, let the ground space $\mathcal{X} = \{x_1, \dots, x_N\}$ be finite and equipped with a metric $d: \mathcal{X} \times \mathcal{X} \rightarrow \mathbb{R}_{\geq 0}$. The OT between two probability distributions on \mathcal{X} then turns into a finite dimensional linear program. More precisely, let

$$\Delta_N := \left\{ r \in \mathbb{R}_{>0}^N \mid \sum_{i=1}^N r_i = 1 \right\}$$

the N -dimensional simplex of fully supported probability distributions on \mathcal{X} . The cost to transport one unit from x_i to x_j is defined by the underlying metric and usually represented by a matrix. For notational convenience we write it as a vector $c \in \mathbb{R}^{N^2}$ with entries $c_{(i-1)N+j} := d^p(x_i, x_j)$ for $p \geq 1$. The OT between the probability distributions $r, s \in \Delta_N$ on \mathcal{X} then amounts to solve the standard linear program

$$\begin{aligned} & \min_{\pi \in \mathbb{R}^{N^2}} \langle c, \pi \rangle \\ & \text{subject to} \quad A\pi = \begin{bmatrix} r \\ s \end{bmatrix}, \pi \geq 0. \end{aligned} \tag{1.1}$$

The coefficient matrix

$$A := \begin{bmatrix} I_{N \times N} \otimes \mathbb{1}_{1 \times N} \\ \mathbb{1}_{1 \times N} \otimes I_{N \times N} \end{bmatrix} \in \mathbb{R}^{2N \times N^2},$$

where \otimes denotes the Kronecker product, encodes the marginal constraints for any transport plan $\pi \in \mathbb{R}^{N^2}$ so that considered as a $N \times N$ matrix its row and column sums are equal to r and s , respectively. In total, the linear program (1.1) consists of $2N$ linear equality constraints in N^2 unknowns. An optimal solution of (1.1) denoted as $\pi_0(r, s)$ (not necessarily unique) is known as an *optimal transport plan*. The quantity

$$W_p(r, s) := \langle c, \pi_0(r, s) \rangle^{\frac{1}{p}}, \tag{1.2}$$

that is the p -th root of the optimal value of (1.1), is referred to as the OT distance, Kantorovich-Rubinstein distance, earth mover's distance or p -th

Wasserstein distance between the probability distributions r and s . Despite its conceptual appeal and its first practical success in various (statistical) applications (Evans and Matsen, 2012; Chernozhukov et al., 2017; Sommerfeld and Munk, 2018; Panaretos and Zemel, 2018), the routine use of OT based data analysis is still lacking as for many real world applications it is severely hindered by its computational burden to solve (1.1). Standard solvers such as the Hungarian method (Kuhn, 1955), the auction algorithm (Bertsekas and Castanon, 1989) or the transportation simplex (Luenberger et al., 1984) require $\mathcal{O}(N^3 \log N)$ steps in the worst case (Pele and Werman, 2009).

There has been made certain progress to overcome this numerical obstacle. For instance, for probability distributions supported on a regular grid equipped with l_1 -distance the OT problem (1.1) can be stated in only $\mathcal{O}(N)$ unknowns as it suffices to consider transport only between neighbouring grid points. This results in an algorithm with average time complexity $\mathcal{O}(N^2)$ (Ling and Okada, 2007). For more general distances Gottschlich and Schuhmacher (2014) introduce the shortlist method, which has been shown empirically to have a runtime of magnitude $\mathcal{O}(N^{2.5})$. Furthermore, multiscale approaches and sparse approximate methods have recently been developed, including Schmitzer (2016a) who solves OT via a sequence of sparse problems. In order to solve the sequence of sparse problems any existing exact transportation algorithm can serve as an internal solver. Empirical simulations demonstrate that current state-of-the-art algorithms, e.g. the transportation simplex, do benefit when applied in a multiscale fashion in terms of memory demand and runtime. However, solving moderately sized problems in reasonable time is still a challenging issue, e.g. in two or three-dimensional imaging, where N is of magnitude $\sim 10^6$ - 10^8 (Schrieber et al., 2017), and large scale problems, such as temporal-spatial image analysis seem currently out of reach.

This encouraged the development of various surrogates for the OT distance which are computationally better accessible. We mention thresholding of the full distance leading to graph sparsification (Pele and Werman, 2009), relaxation (Ferradans et al., 2014) and regularized OT distances (Dessein et al., 2016; Essid and Solomon, 2017). Among the most prominent proposals for the latter approach is the entropy regularization of OT (Cuturi, 2013; Peyré et al., 2017). Instead of solving the linear program (1.1), the entropy regularization approach asks to solve for a positive regularization parameter

$\lambda > 0$ the regularized OT problem

$$\begin{aligned} & \min_{\pi \in \mathbb{R}^{N^2}} \langle c, \pi \rangle + \lambda f(\pi) \\ & \text{subject to } A\pi = \begin{bmatrix} r \\ s \end{bmatrix}. \end{aligned} \tag{1.3}$$

The function $f: \mathbb{R}^{N^2} \rightarrow \mathbb{R}$ is the negative Boltzmann-Shannon entropy defined for $\pi \in \mathbb{R}^{N^2}$ as

$$f(\pi) := \begin{cases} \sum_{i=1}^{N^2} \pi_i \log(\pi_i) - \pi_i + 1 & \text{for } \pi \in \mathbb{R}_{\geq 0}^{N^2}, \\ +\infty & \text{otherwise} \end{cases} \tag{1.4}$$

with the convention $0 \log(0) = 0$. Different to (1.1), the regularization in (1.3) avoids the non-negativity constraint $\pi \geq 0$ since introducing entropy in the objective already enforces any feasible solution to be non-negative. Moreover, the regularized OT (1.3) is a strictly convex optimization program and hence has a *unique* optimal solution $\pi_{\lambda, f}(r, s)$ denoted as *entropy regularized transport plan*. The entropy regularized transport distance, also known as p -th Sinkhorn divergence (Cuturi, 2013), is then defined as

$$W_{p, \lambda, f}(r, s) := \langle c, \pi_{\lambda, f}(r, s) \rangle^{\frac{1}{p}}. \tag{1.5}$$

The major benefit of entropy regularization is of algorithmic nature. The entropy regularized transport plan can be approximated by the Sinkhorn-Knopp algorithm originally introduced by Sinkhorn (1964) that has a linear convergence rate and only requires $\mathcal{O}(N^2)$ operations in each step (Cuturi, 2013). It has been argued that as the regularization parameter $\lambda > 0$ decreases to zero in (1.3) this approximates the solution of the OT problem and hence serves as a good proxy. Nevertheless, high accuracy is hindered by severe numerical limitations in small regularization regimes (Benamou et al., 2015; Schmitzer, 2016b). Furthermore, the runtime of these algorithms typically scales with λ^{-3} (Altschuler et al., 2017; Abid and Gower, 2018).

The results of this paper complement these *computational* findings for regularized OT, as we will show a substantially different *statistical* behaviour compared to (non-regularized) OT ($\lambda = 0$) when the probability distributions r and s are estimated from data, hence randomly perturbed.

To this end and as often typical in applications, the underlying population measure r (resp. s or both) is estimated from given data by its empirical version

$$\hat{r}_n = \frac{1}{n} \sum_{i=1}^n \delta_{X_i}, \quad \left(\hat{s}_m = \frac{1}{m} \sum_{i=1}^m \delta_{Y_i} \right) \tag{1.6}$$

derived by a sample of \mathcal{X} -valued random variables $X_1, \dots, X_n \stackrel{i.i.d.}{\sim} r$ (resp. $Y_1, \dots, Y_m \stackrel{i.i.d.}{\sim} s$). This naturally leads to the question of how the random quantities $\pi_{\lambda, f}(\hat{r}_n, s)$ and $W_{p, \lambda, f}(\hat{r}_n, s)$ behave compared to their population versions $\pi_{\lambda, f}(r, s)$ and $W_{p, \lambda, f}(r, s)$, respectively. In this paper, we provide such an analysis for both quantities by explicitly computing their limit distributions (after proper standardization). Notably, we make use of the fact that entropy regularization (1.3) enforces a *dense* structure for its entropy regularized transport plan, i.e. all its entries are positive. This property, long known and favoured, for instance, in traffic prediction (Wilson, 1969) facilitates our sensitivity analysis for regularized OT (Theorem 2.3). In fact, our approach is different to the technique used in Sommerfeld and Munk (2018) and fails for (non-regularized) OT (1.1) as the optimal (non-regularized) transport plan is known to be sparse.

Our main result (Theorem 3.1) concerns the empirical regularized transport plan itself. More precisely, for $\lambda > 0$ in (1.3) the random quantity $\pi_{\lambda, f}(\hat{r}_n, s)$ converges in distribution (\xrightarrow{D}) to a N^2 -dimensional Gaussian law

$$\sqrt{n} \{ \pi_{\lambda, f}(\hat{r}_n, s) - \pi_{\lambda, f}(r, s) \} \xrightarrow{D} \mathcal{N}_{N^2} (0, \Sigma_{\lambda, f}(r|s)) , \quad (1.7)$$

as $n \rightarrow \infty$. The covariance $\Sigma_{\lambda, f}(r|s)$ depends on λ , the Hessian of the regularization function f and the probability distributions r and s (see (3.1)). Furthermore, the empirical regularized transport distance (1.5) asymptotically follows a centered Gaussian limit law (Theorem 3.2), that is

$$\sqrt{n} \{ W_{p, \lambda, f}(\hat{r}_n, s) - W_{p, \lambda, f}(r, s) \} \xrightarrow{D} \mathcal{N}_1 (0, \sigma_{p, \lambda, f}^2(r|s)) . \quad (1.8)$$

Our results hold true for $r = s$ and $r \neq s$ as well as for other cost vectors c (see Remark 2.4) and are valid for a broad class of regularizers f in (1.3). These will be denoted as *proper regularizers* (Definition 2.2) and subsume various regularization methods of OT (Dessein et al., 2016). Most importantly, it includes the widely applied entropy regularization approach for optimal transport in (1.4) and hence limit distributions for the empirical entropy regularized transport plan and, as a consequence, for the empirical Sinkhorn divergence. For the latter see also Bigot et al. (2017) who obtained limit distributions in a similar fashion to (1.8) for the optimal value of (1.3) with a straightforward application of the technique in Sommerfeld and Munk (2018). Note that the technique we introduce here allows to treat the regularized transport plan itself.

Our findings highlight a substantial difference to related limiting results for *non-regularized* transport. First, and to the best of our knowledge, no distributional limit results are known for the empirical version of the *optimal*

transport plan $\pi_0(\hat{r}_n, s)$, in contrast to the transport distance. Our limit theorems for the regularized transport plan will then be used in Section 4 and Section 7 to derive several statistical consequences. Second, the limit distributions for the regularized transport distance turn out to be substantially different to those of the empirical (non-regularized) OT distance (see Sommerfeld and Munk (2018)) and will not coincide when $\lambda \searrow 0$ in (1.3). In fact, for $r = s$ the empirical (non-regularized) transport distance $W_p(\hat{r}_n, r)$ does not follow asymptotically a Gaussian law, in contrast to (1.8). More precisely, for $p \geq 1$ it holds that

$$n^{1/2p} W_p(\hat{r}_n, r) \xrightarrow{D} \left\{ \max_{u \in \Phi^*} \langle G, u \rangle \right\}^{1/p}, \quad (1.9)$$

as $n \rightarrow \infty$ (Sommerfeld and Munk, 2018). Here, Φ^* is the set of dual solutions for (1.1) and G is a centered N -dimensional Gaussian random vector with covariance matrix

$$\Sigma(r) := \begin{pmatrix} r_1(1-r_1) & -r_1r_2 & \dots & -r_1r_N \\ -r_2r_1 & r_2(1-r_2) & \dots & -r_2r_N \\ \vdots & \vdots & \ddots & \vdots \\ -r_Nr_1 & -r_Nr_2 & \dots & r_N(1-r_N) \end{pmatrix}. \quad (1.10)$$

This different limit behaviour supports the above mentioned computational difficulties to approximate the non-regularized OT distance by the Sinkhorn divergence as $\lambda \searrow 0$.

The outline of this paper is as follows. As a prerequisite for our main methodology and results we provide in Section 2 all necessary terminology from convex optimization. We derive sensitivity results for regularized transport plans which might be of interest by itself as they describe the stability of regularized transport plans when perturbing the boundary conditions given by r and s . Our approach is based on an application of the implicit function theorem to necessary and sufficient optimality conditions for (1.3) with more general regularizers. Parallel to our work, such a sensitivity result was partially obtained by Luise et al. (2018). However, their proof is carried out on the dual formulation of (1.3) and is limited to entropy regularization. Section 3 is dedicated to distributional limit results stated in Theorem 3.1 and Theorem 3.2. Since our proof for (1.7) and (1.8) is based on a delta method, as a byproduct we obtain consistency of the (naive) n out of n bootstrap in Section 4. This is again in notable contrast to the (non-regularized) empirical OT distance, where the (naive) n out of n bootstrap is known to fail (Sommerfeld and Munk, 2018). In Section 5 we investigate in a Monte

Carlo study the speed of convergence of the empirical Sinkhorn divergence sample distribution to its limit distribution. In addition, we investigate the influence of the amount of regularization λ , compare our results to asymptotic distributions for the non-regularized OT distance and investigate the bootstrap empirically.

Section 6 introduces a subsampling method that reduces the computational complexity still inherent in regularization methods, especially for large instant sizes. Finally, in Section 7 we utilize the regularized transport plan and our subsampling method for a statistical analysis of colocalization for protein interaction networks in cells. More precisely, we propose a protocol to analyze the colocalization for images that are beyond the scope of computational feasibility due to their representation by several thousands of pixels. We demonstrate that subsampled colocalization and corresponding confidence bands (see Theorem 7.1) based on the asymptotic law for the empirical regularized transport plan in Theorem 3.1 enable us to make statistical significant statements about the true (population) regularized colocalization. To ease readability all proofs are deferred to the Appendix A.

2 Sensitivity Analysis for Regularized Transport Plans

Optimal transport in its standard form (1.1) can be stated in terms of only $2N - 1$ equality constraints instead of $2N$. In fact, since the total supply equals the total demand ($r, s \in \Delta_N$) any one of the equality constraints is redundant. Without loss of generality we delete the last constraint. Consequently, we define for $r, s \in \Delta_N$ the feasible set for OT as

$$\mathcal{F}(r, s) := \left\{ \pi \in \mathbb{R}_{\geq 0}^{N^2} \mid A_{\star} \pi = [r, s_{\star}]^T \right\} \quad (2.1)$$

with coefficient matrix A_{\star} and vector s_{\star} , where the subscript star denotes the deletion of the last row of the matrix A in (1.1) and the last entry of the vector $s \in \Delta_N$, respectively. This reduction allows for linearly independent constraints described by A_{\star} or equivalently full rank of A_{\star}^T (Luenberger et al., 1984).

Remark 2.1. *In the sequel, we consider OT (1.1) or the entropy regularized OT (1.3) as an optimization program with feasible set $\mathcal{F}(r, s)$ involving A_{\star} and $s_{\star} \in (\Delta_N)_{\star}$. Hence, this requires some caution as we treat r and s asymmetrically.*

We consider regularizers f in (1.3) that are of Legendre type. Legendre-ness means that f is a closed proper convex function on \mathbb{R}^{N^2} which is essentially smooth and strictly convex on the interior of its domain (see e.g. [Dessein et al. \(2016\)](#)). Recall that a function is essentially smooth if it is differentiable on the interior of its domain and for every sequence $(x_k)_{k \in \mathbb{N}} \subset \text{int}(\text{dom } f)$ converging to a boundary point of $\text{int}(\text{dom } f)$ it holds that $\lim_{k \rightarrow \infty} \|\nabla f(x_k)\| = +\infty$. For further details on the class of Legendre functions we refer to [Rockafellar \(1970\)](#).

Definition 2.2 (Proper Regularizer). *Let $f: \mathbb{R}^{N^2} \rightarrow \mathbb{R} \cup \{+\infty\}$ be twice continuously differentiable on the interior of its domain with positive definite Hessian $\nabla^2 f$. Moreover, assume for f and its Fenchel conjugate f^* that*

1. f is of Legendre type,
2. $\mathbb{R}_-^{N^2} \subset \text{dom } f^*$,
3. $(0, 1)^{N^2} \subseteq \text{dom } f$,
4. $\text{dom } f \subseteq \mathbb{R}_{\geq 0}^{N^2}$.

Then f is said to be a proper regularizer.

The examples for proper regularizers are discussed more carefully in the next subsection. By strict convexity, for each proper regularizer f and regularization parameter $\lambda > 0$, we obtain a *unique* regularized transport plan

$$\pi_{\lambda, f}(r, s) = \arg \min_{\pi \in \mathcal{F}(r, s)} \langle c, \pi \rangle + \lambda f(\pi). \quad (2.2)$$

As the main contribution of this section, we focus on *sensitivity analysis* in nonlinear programming, i.e. we investigate how the regularized transport plan $\pi_{\lambda, f}(r, s)$ changes when perturbing the marginal constraints given by $r, s \in \Delta_N$. For a general introduction to sensitivity analysis we refer to [Fiacco \(1984\)](#).

Theorem 2.3. *Let f be a proper regularizer, $r_0, s_0 \in \Delta_N$ and $\lambda > 0$.*

- (a) *The regularized transport plan $\pi_{\lambda, f}(r_0, s_0)$ in (2.2) is unique and contained in the positive orthant $\mathbb{R}_{> 0}^{N^2}$.*
- (b) *There exists a neighbourhood $\mathcal{U} \subseteq \Delta_N \times (\Delta_N)_*$ of (r_0, s_{0*}) and a unique continuously differentiable function*

$$\phi_{\lambda, f}: \mathcal{U} \rightarrow \mathbb{R}^{N^2}$$

such that $\phi_{\lambda,f}(r_0, s_{0\star}) = \pi_{\lambda,f}(r_0, s_0)$. Moreover, the regularized transport plan is parametrized by $\phi_{\lambda,f}$ for all $(r, s_\star) \in \mathcal{U}$ with derivative at $(r_0, s_{0\star})$ given by

$$\nabla\phi_{\lambda,f}(r_0, s_{0\star}) = [\nabla^2 f(\pi_{\lambda,f}(r_0, s_0))]^{-1} A_\star^T [A_\star [\nabla^2 f(\pi_{\lambda,f}(r_0, s_0))]^{-1} A_\star^T]^{-1}$$

a matrix of size $N^2 \times (2N - 1)$.

The crucial observation in our proof (see Appendix A.1) is that proper regularizers enforce the regularized transport plan $\pi_{\lambda,f}$ to be dense, i.e. contained in the positive orthant. Hence, from an optimization point of view the only binding constraints (constraints fulfilled with equality at the optimal solution) are given by the row and column sum requirement, i.e.

$$A_\star \pi = \begin{bmatrix} r \\ s_\star \end{bmatrix}.$$

The gradients of these constraints with respect to π are linearly independent by full rank of A_\star^T , a property well-known as the *linear independence constraint qualification*.

Besides the uniqueness issue in (non-regularized) OT, mimicking the proof for $\lambda = 0$ does not work as we require knowledge about the binding constraints additionally inherent in $\pi \geq 0$. The linear independence constraint qualification fails to hold especially in the case where $\pi_0(r, s)$ consists of more than $2N - 1$ zeroes, a situation known in linear programming as degeneracy of the OT (1.1) (see Luenberger et al. (1984)).

Remark 2.4. *Theorem 2.3 holds independent of the choice for a non-negative cost vector c . However, as we are interested in the regularized transport distance, we restrict ourselves in the subsequent analysis usually to the case that $c_{(i-1)N+j} := d^p(x_i, x_j)$ for $p \geq 1$. Furthermore, Theorem 2.3 implicitly covers different number of support points of the probability distributions r and s which amounts to the situation that, e.g., the probability distribution r does not need to have full support. In such a case, we simply delete the zero entries and our sensitivity result holds for the reduced problem.*

2.1 Proper Regularizers

The class of proper regularizers in Definition 2.2 is rather rich and some common ones are the negative Boltzmann-Shannon entropy (1.4) or l_p quasi

norms ($0 < p < 1$) defined as $f(\pi) = \sum_{i=1}^{N^2} \pi_i^p$ for $\pi \in \mathbb{R}_{\geq 0}$ among others. Further examples that have also been the focus of recent research (Dessein et al., 2016) are given in Table 1. Moreover, we give their Hessians which are required for the sensitivity analysis (Theorem 2.3).

Table 1: Proper regularizers.

Regularizer f	dom f/f^*	$\nabla^2 f$
Boltzmann-Shannon entropy $\sum_{i=1}^{N^2} \log(\pi_i)\pi_i - \pi_i + 1$	$\mathbb{R}_{\geq 0}^{N^2}/\mathbb{R}^{N^2}$	$\text{diag}(\frac{1}{\pi})$
Burg entropy $\sum_{i=1}^{N^2} \pi_i - \log(\pi_i) - 1$	$\mathbb{R}_{> 0}^{N^2}/(-\infty, 1)^{N^2}$	$\text{diag}(\frac{1}{\pi^2})$
Fermi-Dirac entropy $\sum_{i=1}^{N^2} \log(\pi_i)\pi_i + (1 - \pi_i) \log(1 - \pi_i)$	$[0, 1]^{N^2}/\mathbb{R}^{N^2}$	$\text{diag}(\frac{1}{(1-\pi)\pi})$
β -potentials ($0 < \beta < 1$) $\frac{1}{\beta(\beta-1)} \sum_{i=1}^{N^2} \pi_i^\beta - \beta\pi_i + \beta - 1$	$\mathbb{R}_{\geq 0}^{N^2}/(-\infty, \frac{1}{1-\beta})^{N^2}$	$\text{diag}(\pi^{\beta-2})$
l_p quasi norms ($0 < p < 1$) $-\sum_{i=1}^{N^2} \pi_i^p$	$\mathbb{R}_{\geq 0}^{N^2}/\mathbb{R}_{\leq 0}^{N^2}$	$p(1-p)\text{diag}(\pi^{p-2})$

Example 2.5. *If f is the negative Boltzmann-Shannon entropy in (1.4), then the gradient of the parametrization for the entropy regularized transport plan $\pi_{\lambda,f}(r, s)$ is given by*

$$\nabla \phi_{\lambda,f}(r, s_\star) = D A_\star^T [A_\star D A_\star^T]^{-1},$$

where $D \in \mathbb{R}^{N^2 \times N^2}$ is a diagonal matrix with diagonal $\pi_{\lambda,f}(r, s)$.

However, we would like to stress that not all common regularizers fall into the class of proper regularizers.

Example 2.6 (A counterexample). *If f is the l_p norm $1 \leq p < +\infty$, Theorem 2.3 does not hold since f is not a proper regularizer. Moreover, such*

a regularizer allows for a sparse regularized transport plan (Blondel et al., 2017). In particular, we cannot guarantee that its corresponding regularized OT satisfies the linear independence constraint qualification (see discussion after Theorem 2.3). Hence, our proof strategy for l_p ($p \geq 1$) regularized transport plans fails.

3 Distributional Limits

For two probability distributions $r, s \in \Delta_N$, parameter $\lambda > 0$ and proper regularizer f an estimator for $\pi_{\lambda, f}(r, s)$ in (2.2) is given by its empirical counterpart $\pi_{\lambda, f}(\hat{r}_n, s)$ with \hat{r}_n the empirical distribution of the i.i.d. sample X_1, \dots, X_n in (1.6).

The next theorem states a Gaussian limit distribution for the empirical regularized transport plan. Since the sensitivity result in Theorem 2.3 holds regardless of $r = s$ or $r \neq s$ and as the regularized transport plan is always dense, we do not derive any substantial difference regarding statistical limit behaviour in either of these cases.

Theorem 3.1. *Let $r, s \in \Delta_N$ be two probability distributions on the finite metric space (\mathcal{X}, d) and let $X_1, \dots, X_n \stackrel{i.i.d.}{\sim} r$ and \hat{r}_n be the empirical version given in (1.6). Then, as the sample size n grows to infinity, it holds that*

$$\sqrt{n} \{ \pi_{\lambda, f}(\hat{r}_n, s) - \pi_{\lambda, f}(r, s) \} \xrightarrow{D} \mathcal{N}_{N^2}(0, \Sigma_{\lambda, f}(r|s))$$

with covariance matrix

$$\Sigma_{\lambda, f}(r|s) = \nabla_r \phi_{\lambda, f}(r, s_*) \Sigma(r) [\nabla_r \phi_{\lambda, f}(r, s_*)]^T, \quad (3.1)$$

where $\Sigma(r)$ is defined in (1.10) and $\nabla_r \phi_{\lambda, f}(r, s_*)$ are the partial derivatives of $\phi_{\lambda, f}$ with respect to r as given in Theorem 2.3.

The proof is based on the multivariate delta method and can be found in the Appendix A.2. Further, we show for $\lambda > 0$ and a proper regularizer f limit distributions for the empirical counterpart of the regularized transport distance (1.5). Here, s (which might be equal to r) plays the role of a fixed reference probability distribution to be compared empirically with the probability distribution r .

The proof is an application of the delta method in conjunction with the limit law from Theorem 3.1. We again do not derive any substantially different distributional limit behaviour between the cases $r = s$ and $r \neq s$. This is in notably contrast to the non-regularized OT (see the discussion in the introduction and Section 3.2).

Theorem 3.2. *Under the assumptions of Theorem 3.1, as $n \rightarrow \infty$ it holds that*

$$\sqrt{n} \{W_{p,\lambda,f}(\hat{r}_n, s) - W_{p,\lambda,f}(r, s)\} \xrightarrow{D} \mathcal{N}_1(0, \sigma_{p,\lambda,f}^2(r|s))$$

with variance

$$\sigma_{p,\lambda,f}^2(r|s) = \gamma^T \Sigma_{\lambda,f}(r|s) \gamma, \quad (3.2)$$

where γ is the gradient of the function $\pi \mapsto \langle c, \pi \rangle^{\frac{1}{p}}$ evaluated at the regularized transport plan $\pi_{\lambda,f}(r, s)$ and $\Sigma_{\lambda,f}(r|s)$ is the covariance matrix from Theorem 3.1. Standardizing by the square root of the empirical variance $\sigma_{p,\lambda,f}^2(\hat{r}_n|s)$ results in a standard normal limit distribution.

The proof is included in the Appendix A.3. As a corollary, we immediately obtain limit distributions for the entropy empirical regularized transport plan and the empirical Sinkhorn divergence.

Corollary 3.3 (Sinkhorn transport and Sinkhorn divergence). *Consider the negative Boltzmann-Shannon entropy f in (1.4). Then the statements in Theorem 3.1 and Theorem 3.2 remain valid. Note, that for the corresponding covariance matrix (3.1) the gradient is given by Example 2.5.*

Remark 3.4 (Limit behaviour as λ tends to zero). *For f the Boltzmann-Shannon entropy and the case of $N = 2$ support points, i.e. $r = (r_1, 1 - r_1) \in \Delta_2$ and $s = (s_1, 1 - s_1) \in \Delta_2$ with cost $c = (0, c_1, c_1, 0)^T$ for $c_1 \in \mathbb{R}_{\geq 0}$, cumbersome computations yield that $\lim_{\lambda \searrow 0} \sigma_{1,\lambda,f}^2(r|r) = 0$. Hence, the limit of*

$$\sqrt{n} \{W_{1,\lambda,f}(\hat{r}_n, s) - W_{1,\lambda,f}(r, s)\} \quad (3.3)$$

for λ to zero is a Dirac measure at zero. This limit behaviour can be interpreted as a randomized stability analysis. It is known that the Sinkhorn divergence numerically approximates the OT distance as λ tends to zero. However, (3.3) does not approximate the limit distribution for (non-regularized) transport in (1.9) which clearly is not equal to a Dirac measure at zero. This difference also highlights recent findings by Altschuler et al. (2017) who proves that the computational complexity scales with λ^{-3} . Hence, also from a numerical point of view a degeneracy occurs. Nevertheless, for $r \neq s$ we find that

$$\lim_{\lambda \searrow 0} \sigma_{1,\lambda,f}^2(r|s) = c_1^2 r_1 (1 - r_1),$$

which is precisely the variance of the centered normal distribution for (non-regularized) transport distance for $r \neq s$ under non-degeneracy (Sommerfeld, 2017a, Section 2.6). Numerical computations suggest that this holds true for general $N \in \mathbb{N}$.

3.1 Estimating Both Probability Distributions

Theorem 3.1 and Theorem 3.2 also hold true when we estimate both distributions r and s . More precisely, we estimate the distributions by their empirical versions \hat{r}_n and \hat{s}_m in (1.6) derived by two collections of \mathcal{X} -valued random variables $X_1, \dots, X_n \stackrel{i.i.d.}{\sim} r$ and independently $Y_1, \dots, Y_m \stackrel{i.i.d.}{\sim} s$, respectively.

Following essentially the same arguments as before we derive limit distributions for the empirical regularized transport plan $\pi_{\lambda, f}(\hat{r}_n, \hat{s}_m)$ and for the empirical regularized transport distance $W_{p, \lambda, f}(\hat{r}_n, \hat{s}_m)$. Note that we treat r and s asymmetrically (see Remark 2.1). Hence, the underlying multinomial process is based on the reduced multinomial vector (r, s_\star) rather than (r, s) . The scaling rate is given by $\sqrt{\frac{nm}{n+m}}$ such that $n \wedge m \rightarrow +\infty$ and $\frac{m}{n+m} \rightarrow \delta \in (0, 1)$.

For instance, the limit distribution for the empirical regularized transport plan with parameter $\lambda > 0$ and proper regularizer f then reads as

$$\sqrt{\frac{nm}{n+m}} \{ \pi_{\lambda, f}(\hat{r}_n, \hat{s}_m) - \pi_{\lambda, f}(r, s) \} \xrightarrow{D} \mathcal{N}_{N^2}(0, \Sigma_{\lambda, f}(r, s)).$$

The variance $\Sigma_{\lambda, f}(r, s)$ is different to $\Sigma_{\lambda, f}(r|s)$ from Theorem 3.1. More precisely, given the covariance matrix of the reduced multinomial process

$$\Sigma(\delta, r, s_\star) = \begin{pmatrix} \delta \Sigma(r) & 0 \\ 0 & (1 - \delta) \Sigma(s_\star) \end{pmatrix},$$

we find that

$$\Sigma_{\lambda, f}(r, s) = \nabla \phi_{\lambda, f}(r, s_\star) \Sigma(\delta, r, s_\star) \nabla \phi_{\lambda, f}(r, s_\star)^T. \quad (3.4)$$

Similar the limit distribution for the empirical regularized transport distance with parameter $\lambda > 0$ and proper regularizer f now reads as

$$\sqrt{\frac{nm}{n+m}} \{ W_{p, \lambda, f}(\hat{r}_n, \hat{s}_m) - W_{p, \lambda, f}(r, s) \} \xrightarrow{D} \mathcal{N}_1(0, \sigma_{p, \lambda, f}^2(r, s)).$$

The variance $\sigma_{p, \lambda, f}^2(r, s)$ again is different to $\sigma_{p, \lambda, f}^2(r|s)$ from Theorem 3.2 and given as

$$\sigma_{p, \lambda, f}^2(r, s) = \gamma^T \Sigma_{\lambda, f}(r, s) \gamma,$$

where we recall the definition of γ from Theorem 3.2.

3.2 Scaling Behaviour for Higher Order Regularized Transport Distances

We highlight here that as a common property all delta type methods respect the scaling rate of the underlying process. Hence, the scaling rate for limit laws for the empirical p -th regularized transport distance is \sqrt{n} independent of the order $p \geq 1$. However, according to (1.9) for $r = s$ the scaling rate for empirical p -th Wasserstein distances is given by $n^{1/2p}$ (see Sommerfeld and Munk (2018)). While the rate for the empirical (non-regularized) p -th Wasserstein distance is easily seen to be a consequence of the continuous mapping theorem, this approach fails for its regularized version as $W_{p,\lambda,f}(r, r) > 0$.

4 Bootstrap

The (non-regularized) transport distance on finite spaces defines a functional that is only *directionally* Hadamard differentiable, i.e. has a *non-linear* derivative with respect to r and s . Hence, the (naive) n out of n bootstrap method to approximate the distributional limits for the (non-regularized) empirical transport distance fails (Sommerfeld and Munk, 2018). However, our arguments underlying the proof of Theorem 3.1 for the regularized transport are based on the usual delta method for *linear* derivatives. As a byproduct we obtain that for the regularized transport plan and for the regularized transport distance the n out of n bootstrap is consistent. More precisely, conditionally on the data X_1, \dots, X_n , the law of the multinomial empirical bootstrap process $\sqrt{n}\{\hat{r}_n^* - \hat{r}_n\}$ is an asymptotically consistent estimator of the law for the multinomial empirical process $\sqrt{n}\{\hat{r}_n - r\}$ (van der Vaart and Wellner, 1996, Theorem 3.6.1). Here, $\hat{r}_n^* = \frac{1}{n} \sum_{i=1}^n \delta_{X_i^*}$ is the empirical bootstrap estimator for \hat{r}_n derived by a sample $X_1^*, \dots, X_n^* \stackrel{i.i.d.}{\sim} \hat{r}_n$. Such conditional weak convergence can be formulated in terms of the bounded Lipschitz metric, that is

$$\sup_{h \in \text{BL}_1(\mathbb{R}^N)} |\mathbb{E}[h(\sqrt{n}\{\hat{r}_n^* - \hat{r}_n\}) | X_1, \dots, X_n] - \mathbb{E}[h(\sqrt{n}\{\hat{r}_n - r\})]| \quad (4.1)$$

converges to zero in probability, where

$$\text{BL}_1(\mathbb{R}^N) := \left\{ f: \mathbb{R}^N \rightarrow \mathbb{R} \mid \sup_{x \in \mathbb{R}^N} |f(x)| \leq 1, |f(x_1) - f(x_2)| \leq \|x_1 - x_2\| \right\}$$

is the set of all bounded functions with Lipschitz constant at most one. Combined with the consistency of the delta method for the bootstrap (van der

Vaart and Wellner, 1996, Theorem 3.9.11), this proves the consistency for the entropy regularized empirical bootstrap transport plan. The statements again hold true for $r = s$ and $r \neq s$.

Theorem 4.1. *Under the assumptions of Theorem 3.1 the (naive) bootstrap for the regularized transport plan is consistent, that is*

(a)

$$\begin{aligned} & \sup_{h \in BL_1(\mathbb{R}^{N^2})} |\mathbb{E}[h(\sqrt{n} \{\pi_{\lambda,f}(\hat{r}_n^*, s) - \pi_{\lambda,f}(\hat{r}_n, s)\}) | X_1, \dots, X_n] \\ & \quad - \mathbb{E}[h(\sqrt{n} \{\pi_{\lambda,f}(\hat{r}_n, s) - \pi_{\lambda,f}(r, s)\})]|] \xrightarrow{\mathbb{P}} 0. \end{aligned}$$

This holds as well for the p -th regularized transport distance

(b)

$$\begin{aligned} & \sup_{h \in BL_1(\mathbb{R})} |\mathbb{E}[h(\sqrt{n} \{W_{p,\lambda,f}(\hat{r}_n^*, s) - W_{p,\lambda,f}(\hat{r}_n, s)\}) | X_1, \dots, X_n] \\ & \quad - \mathbb{E}[h(\sqrt{n} \{W_{p,\lambda,f}(\hat{r}_n, s) - W_{p,\lambda,f}(r, s)\})]|] \xrightarrow{\mathbb{P}} 0. \end{aligned}$$

Analogously, the bootstrap consistency is valid if $Y_1^*, \dots, Y_m^* \stackrel{i.i.d.}{\sim} \hat{s}_m^*$ independently to $X_1^*, \dots, X_n^* \stackrel{i.i.d.}{\sim} \hat{r}_n^*$ (see Section 3).

5 Simulations

We illustrate our distributional limit results in Monte Carlo simulations. Exemplarily, we investigate the speed of convergence for the empirical Sinkhorn divergence ($p = 1$) to its limit distribution (Corollary 3.3) in the one-sample case in both settings $r = s$ and $r \neq s$. Moreover, we illustrate the accuracy of approximation by the (naive) n out of n bootstrap (Theorem 4.1). As the Sinkhorn divergence approximates the (non-regularized) OT distance, we also compare for small regularization parameters the finite sample distribution of the Sinkhorn divergence with the limit laws for the (non-regularized) optimal transport distance (OT distance) in (1.9).

All simulations were performed using R (R Core Team, 2016). The Sinkhorn divergences are calculated with the R-package *Barycenter* (Klatt, 2018).

Remark 5.1 (Computation of (empirical) variances). For $p = 1$ it holds that $\sigma_{1,\lambda,f}^2(r|s) = c^T \Sigma_{\lambda,f}(r|s) c$. According to Example 2.5 and Corollary 3.3, the computation of the variance involves the computation of

$$\begin{aligned} \Sigma_{\lambda,f}(r|s) &= \nabla_r \phi_{\lambda,f}(r, s_\star) \Sigma(r) [\nabla_r \phi_{\lambda,f}(r, s_\star)]^T \\ &= D A_\star^T [A_\star D A_\star^T]_{[1:N]}^{-1} \Sigma(r) [A_\star D A_\star^T]_{[1:N]}^{-1} A_\star D, \end{aligned}$$

where the subscript notation $[1 : N]$ denotes the first N columns of the corresponding matrix. Recall that D is equal to a diagonal matrix with diagonal given by the entropy regularized transport plan $\pi_{\lambda,f}(r, s)$ and A_\star is the coefficient matrix in (1.1) reduced by its last row. Besides calculating the regularized transport plan, the computation of the variance faces matrix inversion. However, the matrix $A_\star D A_\star^T$ is symmetric and positive definite by full rank of A_\star . Moreover, it posses a block structure given by

$$A_\star D A_\star^T = \begin{bmatrix} R & \Pi_{\lambda,f} \\ \Pi_{\lambda,f}^T & S_\star \end{bmatrix},$$

where $\Pi_{\lambda,f}$ denotes the matrix version of the regularized transport plan reduced by its last column, and we set $R := \text{diag}(r)$ and $S_\star := \text{diag}(s_\star)$. Hence, we can apply a block wise inversion and obtain

$$[A_\star D A_\star^T]_{[1:N]}^{-1} = \begin{bmatrix} [R - \Pi_{\lambda,f} S_\star^{-1} \Pi_{\lambda,f}^T]^{-1} \\ -S_\star^{-1} \Pi_{\lambda,f}^T [R - \Pi_{\lambda,f} S_\star^{-1} \Pi_{\lambda,f}^T]^{-1} \end{bmatrix}.$$

We consider the finite metric space \mathcal{X} to be an equidistant two-dimensional $L \times L$ grid on $[0, 1] \times [0, 1]$ and the cost $c \in \mathbb{R}^{L^2}$ consisting of the euclidean distance ($p = 1$) between the pixels on the grid. Note that different grid sizes for fixed regularization parameter λ correspond to different amounts of regularization. As recommended by Cuturi (2013), we let the amount of regularization depend on the median distance $q_{50}(c)$ between the pixels on the grid. More precisely, we define the regularization parameter by

$$\lambda := \lambda_0 q_{50}(c), \quad (5.1)$$

where $\lambda_0 > 0$ is a parameter that we vary for different simulations. The probability distributions $r, s \in \Delta_{L^2}$ on \mathcal{X} are generated as two independent realizations of a Dirichlet random variable $\text{Dir}(\alpha)$ with concentration parameter $\alpha = (\alpha, \dots, \alpha) \in \mathbb{R}^{L \times L}$. We choose $\alpha = 1$ corresponding to a uniform distribution on the probability simplex Δ_{L^2} .

5.1 Speed of Convergence

We first generate for grid size $L = 10$ two probability distributions r, s on \mathcal{X} as two independent realizations of a Dirichlet random variable $\text{Dir}(\mathbf{1})$, respectively. We fix the amount of regularization to $\lambda = 2q_{50}(c)$, that is $\lambda_0 = 2$ in (5.1). We then sample $n = 25$ observations according to the probability distribution r and generate 20.000 realizations, referred to as Sinkhorn samples, for $r = s$ of

$$\sqrt{\frac{n}{\sigma_{1,\lambda,f}^2(\hat{r}_n | r)}} \{W_{1,\lambda,f}(\hat{r}_n, r) - W_{1,\lambda,f}(r, r)\},$$

that is when the data generating probability distribution r coincides with the probability distribution to be compared. Similar, we consider the same set up in the case $r \neq s$. The finite sample distributions are then compared to their theoretical limit distributions which by Theorem 3.2 are standard normal distributions.

We demonstrate the results by kernel density estimators and corresponding Q-Q-plots in the first row of Figure 1 (a) and (b). We observe that the finite sample distribution is already well approximated for small sample size ($n = 25$) by the theoretical limit distribution. However, the amount of entropy regularization ($\lambda_0 = 2$) added to OT is rather large. We find that for sample size $n = 25$ the smaller the regularization λ_0 the worse the approximation by the theoretical Gaussian limit law. This is depicted in the second row of Figure 1 (a) and (b) where we analyze for small regularization parameters the Kolmogorov-Smirnov distance (maximum absolute difference between empirical cdf and cdf of the limit law). Note, that the theoretical limit law approximates the finite sample distribution slightly better in the case $r \neq s$.

We additionally investigate the speed of convergence with respect to the Kolmogorov-Smirnov distance of the finite sample distribution in the small regularization regime when the sample size is large ($n \gg 25$). As illustrated in Figure 2 we observe in our simulations good approximation results for rather large regularization whereas for small regularization the approximation accuracy decreases. This can only be compensated if the sample size n severely increases to several thousands. As a benchmark, for $\lambda_0 = 0.2$ we already require $n = 5000$ samples to observe an accurate approximation by the limit distribution from Theorem 3.2.

Motivated by the inaccurate approximation for small sample size in the small regularization regime and the fact that the Sinkhorn divergence converges to the OT distance as $\lambda_0 \searrow 0$, we compare the finite sample distribu-

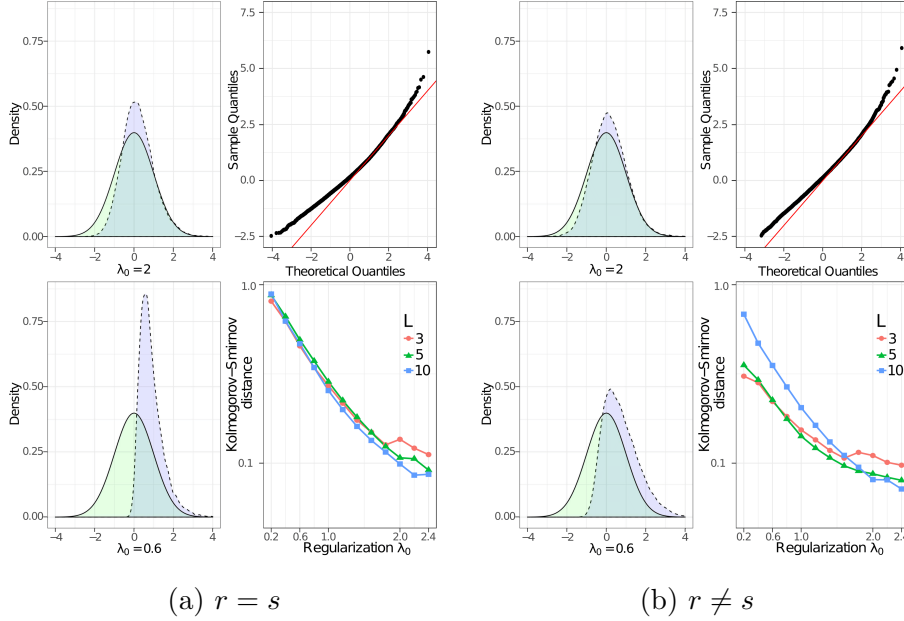


Figure 1: (a) Finite sample accuracy of the limit law in the one sample case for $r = s$. First row: Finite sample density (dashed line) of the empirical Sinkhorn divergence for $n = 25$ on a regular grid of size $L = 10$ with regularization parameter $\lambda_0 = 2$ compared to its limit law (standard Gaussian, solid line). The finite sample density has been estimated with a kernel density estimator with Gaussian kernel and Silverman's rule to select bandwidth. On the right the corresponding Q-Q-plot, where perfect fit is indicated by the red solid line. Second row: L.h.s. same setting as above, $\lambda_0 = 0.6$. R.h.s. Finite sample accuracy in dependence on λ_0 : The Kolmogorov-Smirnov distance averaged over five measures on a logarithmic scale between the finite sample distribution ($n = 25$) of the empirical Sinkhorn divergence and the standard normal distribution as a function of the regularization parameter λ_0 .

(b) Finite sample accuracy of the limit law in the one sample case for $r \neq s$. Same scenario as in (a) whereas here the probability distribution r to be sampled is not equal to the fixed reference probability distribution s .

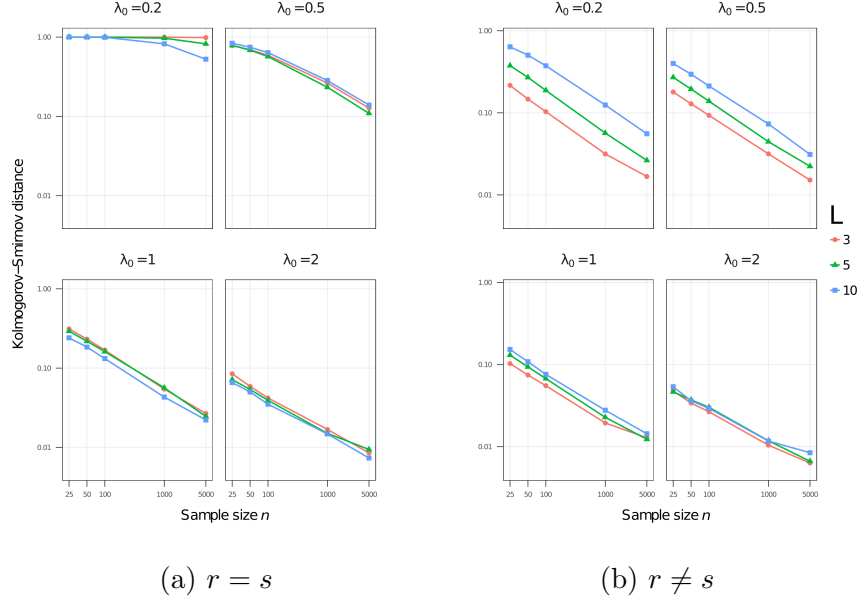


Figure 2: (a) Kolmogorov-Smirnov distance in the one-sample case for $r = s$. The Kolmogorov-Smirnov distance between the finite Sinkhorn divergence sample distribution and its theoretical normal distribution for $r = s$ (left) and $r \neq s$ (right) as a function of the sample size $n \in \{25, 50, 100, 1000, 5000\}$ for different grid sizes $L \times L$ and different regularization parameters λ_0 . The distances are averaged over five pairs of measures. The axes are given on a logarithmic scale.
(b) Kolmogorov-Smirnov distance in the one-sample case for $r \neq s$. Same scenario as in (a) whereas here the probability distribution r to be sampled is not equal to the fixed reference probability distribution s .

tion to the (non-regularized) OT limit law in Sommerfeld and Munk (2018) for the case $r = s$. From Figure 3 we see that the finite sample distribution for $\lambda_0 = 0.1$ and $\lambda_0 = 0.05$ and small sample size ($n = 25$) is approximated by the OT limit law in (1.9).

In summary, the finite sample distribution converges to its theoretical limit law. The accuracy of the approximation is driven by the regularization parameter λ_0 . For large regularization added to OT, the limit law serves as a good approximation to the finite sample distribution, already for small sample sizes and independent of the size of the ground space. As λ_0 decreases, accuracy of approximation decreases. Especially for small sample sizes the finite sample distribution is approximated by the (non-regularized) OT distance limit law in (1.9) than by its theoretical Gaussian limit law.

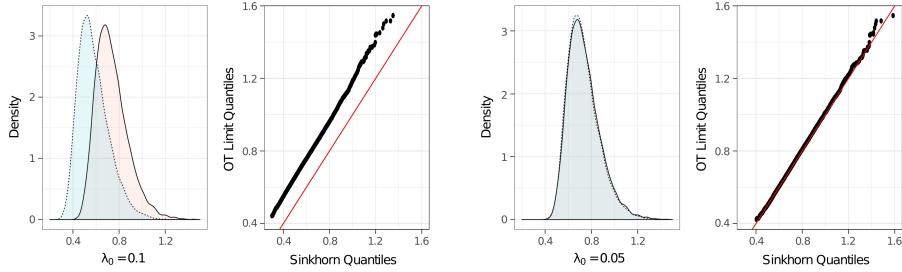


Figure 3: Comparison to OT limit law in the one-sample case for $r = s$. Comparison of the finite sample distribution ($n = 25$) of the empirical Sinkhorn divergence on an equidistant grid of size $L = 10$ for regularization parameter $\lambda_0 = 0.1$ (left two figures) and $\lambda_0 = 0.05$ (right two figures) to the OT limit law in (1.9) (Sommerfeld and Munk, 2018, Theorem 1). Kernel density estimator for the Sinkhorn sample (dotted line) and the OT sample (solid line) with corresponding Q-Q-plot on the right. The OT distance limit distribution is approximated by a sample of size 20.000 implemented in the R-package *otinference* (Sommerfeld, 2017b).

5.2 Simulating the Bootstrap

Additionally, we simulate the (naive) n out of n plug-in bootstrap approximation from Section 4 in the one-sample case for $r = s$. For an equidistant grid with $L = 10$ on $[0, 1] \times [0, 1]$ and cost given by the euclidean distance as before, we generate r as a realization of a Dirichlet random variable $\text{Dir}(\mathbf{1})$ and generate 20.000 realizations

$$\sqrt{n} \{W_{1,\lambda,f}(\hat{r}_n, r) - W_{1,\lambda,f}(r, r)\}, \quad (5.2)$$

where we set the sample size $n = 100$ and as before vary λ_0 . Moreover, for fixed empirical distribution \hat{r}_n and each λ_0 we generate $B = 500$ bootstrap replications

$$\sqrt{n} \{W_{1,\lambda,f}(\hat{r}_n^*, r) - W_{1,\lambda,f}(\hat{r}_n, r)\} \quad (5.3)$$

by drawing independently with replacement $n = 100$ times according to \hat{r}_n . We then compare the finite sample distributions again by kernel density estimators. The results are depicted in Figure 4.

In fact, the finite bootstrap sample distribution is a good approximation of the finite sample distribution. However, as before, the speed of convergence to the corresponding limit distribution is driven by the amount of regularization. Similar results hold for the two-sample case (not displayed).

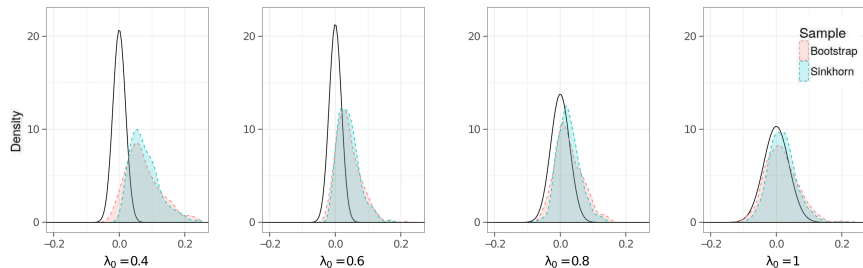


Figure 4: Bootstrap in the one-sample case for $r = s$. Illustration of the (naive) n out of n plug-in bootstrap approximation ($n = 100$) for different regularization parameters λ_0 on a grid of size $L = 10$. The density in blue (resp. red) is obtained by a kernel density estimator (Gaussian kernel with bandwidth given by Silverman’s rule) of a Sinkhorn divergence sample (20.000 realizations) (5.2) (resp. bootstrap sample (5.3), $B = 500$ replications). The density of the corresponding Gaussian limit is depicted in black.

6 Reducing Computational Complexity by Sub-sampling

Altschuler et al. (2017) discuss algorithms for the computation of entropy regularized OT which approximate the OT distance such that

$$W_{1,\lambda,f}(r, s) \leq W_1(r, s) + \epsilon$$

in time $\mathcal{O}(N^2 \log(N) \epsilon^{-3})$. These methods are usually based on matrix scaling of the underlying $N \times N$ distance matrix in order to find the regularized transport plan $\pi_{\lambda,f}(r, s)$ in (2.2). Hence, as soon as the number of support points N of the underlying measures increases matrix scaling becomes computational infeasible mainly because of the high memory demand to store and scale the distance matrix.

In order to maintain computational feasibility, we borrow an idea introduced by Sommerfeld et al. (2018), i.e. we use a subsampling scheme of the underlying probability measures. The subsequent data example in Section 7 requires to deal with probability measures with support on up to $N = 300.000$ points (images represented by normalized gray scale pixel intensities). This requires storing a distance matrix with entries $300.000^2 = 9 \cdot 10^{12}$ which is far beyond the storage capacity of any standard laptop. In order to stay within the scope of computational feasibility we subsample from these probability measures $n = 50.000$ data points which reduces the required storage to $50.000^2 = 2.5 \cdot 10^9$ entries. Note that while the number of support points

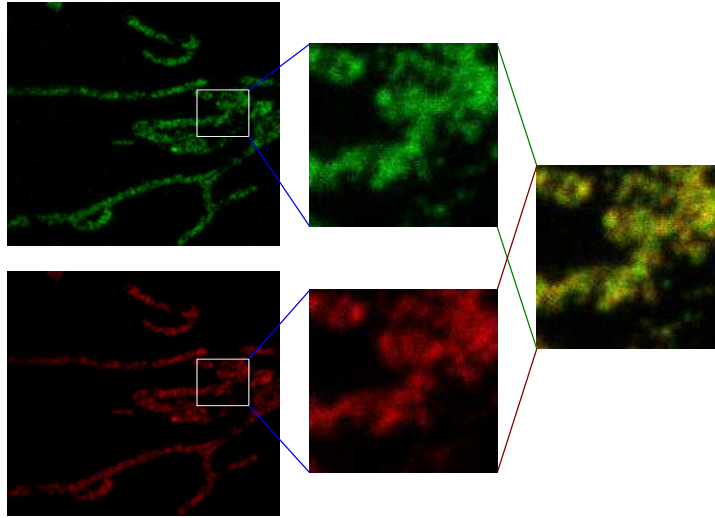
of the subsampled probability measures decreases by a sixth, the memory demand for the corresponding distance matrix is reduced by three orders of magnitude. This is crucial as it keeps matrix scaling feasible.

7 Colocalization Analysis

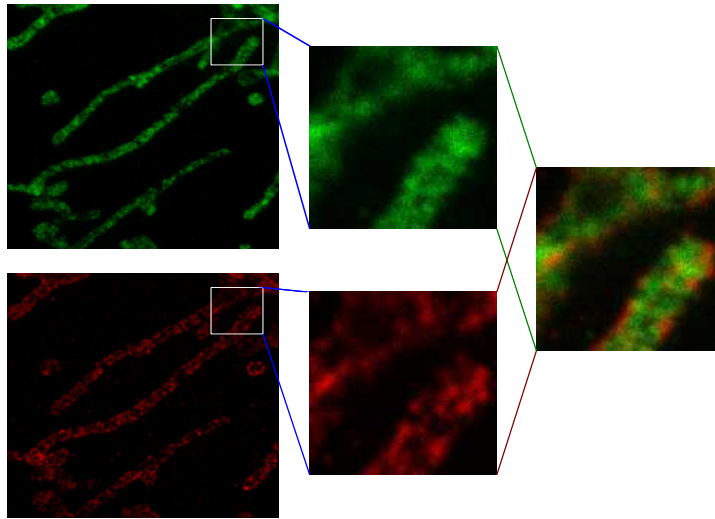
Complex protein interaction networks are at the core of almost all cellular processes. To gain insight into these networks a valuable tool is colocalization analysis of images generated by fluorescence microscopy aiming to quantify the spatial proximity of proteins (Comeau et al., 2006; Adler and Parmryd, 2010; Zinchuk and Grossenbacher-Zinchuk, 2014). With the advent of super-resolution microscopy (nanoscopy) nowadays protein structures at a size of a single protein can be discerned. This challenges conventional colocalization methods, e.g. based on pixel intensity correlation as there is no spatial overlap due to blurring anymore (Xu et al., 2016).

In Figure 5 exemplary 2-color-STED images (recorded at the Jakobs’ lab, Department of NanoBiophotonics, Max-Planck Institute for Biophysical Chemistry, Göttingen) are displayed. These are generated by inserting two different fluorophore markers which emit photons at different wavelength (two colors) and reading them out, after exciting them, with a stimulated emission depletion (STED) laser beam (Hell, 2007). Figure 5 (a) shows 2-color-STED images which were generated by attaching the two markers to the protein *ATP Synthase*. Figure 5 (b) displays the second case in which the markers are attached to two different proteins *ATP Synthase* and *MIC60*. We aim to quantify the spatial proximity of *ATP Synthase* and *MIC60* (Figure 5 (b)) and to set this in relation with the highest empirically possible colocalization represented by the double staining of the protein *ATP Synthase* (Figure 5 (a)). The overlay of the channels from setting two in Figure 5 (b) already indicates that *ATP Synthase* and *MIC60* are located in different regions as there are only small areas which are yellow. In contrast, and as expected for the highest empirically possible colocalization, the yellow areas in the overlay of the two channels from the double staining in Figure 5 (a) are more pronounced.

In this section, we illustrate that the regularized transport plan (2.2) provides a useful tool to measure colocalization in super-resolution images as it finds the (regularized) optimal matching between the two protein intensity distributions. The set of pixels define the ground space $\mathcal{X} = \{x_1, \dots, x_N\}$ with $N = N_x \cdot N_y$, where N_x, N_y are the number of pixels in x - and y -direction, respectively. The pixels color intensities are understood (after



(a) **Setting 1:** Double staining of the protein *ATP Synthase*.



(b) **Setting 2:** Staining of the proteins *ATP Synthase* (green) and *MIC60* (red).

Figure 5: STED images for colocalization analysis. Exemplary STED images of the two colocalization scenarios. Left: Images of a green and a red channel. Image size 666×666 pixels, pixel size = 15nm. Middle: Zoom ins (128×128 pixels). Right: Overlay of zoomed in images.

normalization) as discrete probability measures $r, s \in \Delta_N$ on an equidistant grid in $[0, N_x \cdot l] \times [0, N_y \cdot l]$, where l is the pixel size. The cost to transport pixel intensities from one pixel to the other is given by the squared euclidean distance $c_{(i-1)N+j} = \|x_i - x_j\|^2$ and $c_{\max} := \max_{1 \leq i \leq N^2} c_i$ is the maximal distance on the ground space \mathcal{X} .

We introduce the *regularized colocalization measure* $R\text{Col}$ which is based on the regularized transport plan $\pi_{\lambda, f}(r, s)$ and defined by

$$R\text{Col} := R\text{Col}(\pi_{\lambda, f}(r, s))(\cdot) = \sum_{i=1}^{N^2} \pi_{\lambda, f}(r, s)_i \mathbb{1}\{c_i \leq \cdot\}. \quad (7.1)$$

Intuitively, $R\text{Col}(\pi_{\lambda, f}(r, s))(t)$ for $t \in [0, c_{\max}]$ is the proportion of pixel intensities which is transported on scales smaller or equal to t in the (regularized) optimal matching of the two intensity distributions with respect to some amount of regularization specified by λ . The function $R\text{Col}(\pi)$ constitutes an element in $\mathcal{D}[0, c_{\max}]$ the space of all *càdlàg* functions (Billingsley, 2013) on $[0, c_{\max}]$ equipped with the supremum norm $\|f\|_{\infty} := \sup_{t \in [0, c_{\max}]} |f(t)|$. By definition the map $\pi \mapsto R\text{Col}(\pi)$ is linear and Lipschitz with constant at most one.

Theorem 7.1. *Let $\widehat{R\text{Col}}_n := R\text{Col}(\pi_{\lambda, f}(\hat{r}_n, s))$ be the empirical regularized colocalization. Under the assumptions of Theorem 3.1, as $n \rightarrow \infty$ it holds that*

$$\sqrt{n} \left\{ \widehat{R\text{Col}}_n - R\text{Col} \right\} \xrightarrow{D} R\text{Col}(G),$$

where G is the centered Gaussian random variable in \mathbb{R}^{N^2} with covariance $\Sigma_{\lambda, f}(r|s)$ given in (3.1).

The proof can be found in the Appendix A.4. According to Theorem 7.1 and the continuous mapping theorem, we obtain, as n approaches infinity, that

$$\left\| \sqrt{n} \left\{ \widehat{R\text{Col}}_n - R\text{Col} \right\} \right\|_{\infty} \xrightarrow{D} \|R\text{Col}(G)\|_{\infty}.$$

This result enables us to derive *approximate confidence bands (CBs)* for the regularized colocalization. Let $\mathbf{u}_{1-\alpha}$ be the $1 - \alpha$ quantile from the distribution of $\|R\text{Col}(G)\|_{\infty}$. Hence, for each $\alpha \in (0, 1)$,

$$\mathcal{I}_n := \left[-\frac{\mathbf{u}_{1-\alpha}}{\sqrt{n}} + \widehat{R\text{Col}}_n, \frac{\mathbf{u}_{1-\alpha}}{\sqrt{n}} + \widehat{R\text{Col}}_n \right] \quad (7.2)$$

is a $1 - \alpha$ approximate CB for the regularized colocalization $R\text{Col}$. More precisely, it holds that

$$\lim_{n \rightarrow \infty} \mathbb{P}(R\text{Col} \in \mathcal{I}_n) = 1 - \alpha.$$

In our subsequent data example we require to estimate both probability measures $r, s \in \Delta_N$ (see end of Section 3). The confidence band (7.2) naturally extends to this case. Defining for $n, m \in \mathbb{N}$ the two sample empirical version of the regularized colocalization

$$\widehat{\text{RCol}}_{n,m} := \text{RCol}(\pi_{\lambda,f}(\hat{r}_n, \hat{s}_m)),$$

we have, as the sample size $n \wedge m \rightarrow +\infty$ and $\frac{m}{n+m} \rightarrow \delta \in (0, 1)$, that

$$\sqrt{\frac{nm}{n+m}} \left\{ \widehat{\text{RCol}}_{n,m} - \text{RCol} \right\} \xrightarrow{D} \text{RCol}(G). \quad (7.3)$$

Now, the random variable G is centered Gaussian with covariance matrix $\Sigma_{\lambda,f}(r, s)$ given in (3.4). In particular, for equal sample size $n = m$ the corresponding two sample CB reads as

$$\mathcal{I}_{n,n} := \left[-\frac{\sqrt{2}\mathbf{u}_{1-\alpha}}{\sqrt{n}} + \widehat{\text{RCol}}_{n,n}, \frac{\sqrt{2}\mathbf{u}_{1-\alpha}}{\sqrt{n}} + \widehat{\text{RCol}}_{n,n} \right], \quad (7.4)$$

with $\mathbf{u}_{1-\alpha}$ according to the supremum of the r.h.s. of (7.3).

7.1 Bootstrap Confidence Bands for Colocalization

We denote by $\widehat{\text{RCol}}_{n,n}^*$ a bootstrap version of the regularized colocalization based on the empirical bootstrap estimators \hat{r}_n^* and \hat{s}_n^* derived by bootstrapping from the empirical distributions \hat{r}_n and \hat{s}_n (see Section 4). Note that RCol is Lipschitz and therefore, according to Theorem 4.1 and an application of the continuous mapping theorem for the bootstrap (Kosorok, 2008, Proposition 10.7), we deduce that

$$\begin{aligned} \sup_{h \in \text{BL}_1(\mathbb{R})} & \left| \mathbb{E} \left[h \left(\left\| \sqrt{n/2} \left\{ \widehat{\text{RCol}}_{n,n}^* - \widehat{\text{RCol}}_{n,n} \right\} \right\|_{\infty} \right) \middle| X_1, \dots, X_n, Y_1, \dots, Y_n \right] \right. \\ & \left. - \mathbb{E} \left[h \left(\left\| \sqrt{n/2} \left\{ \widehat{\text{RCol}}_{n,n} - \text{RCol} \right\} \right\|_{\infty} \right) \right] \right| \xrightarrow{\mathbb{P}} 0. \end{aligned}$$

Hence, the quantile $\mathbf{u}_{1-\alpha}$ is consistently approximated by its bootstrap analogon, say $\mathbf{u}_{1-\alpha}^*$. This yields a bootstrap approximation of the CB in (7.4).

7.1.1 Validation of Bootstrap and Subsampling on Real Data

The goal of the following analysis is to investigate the validity of the bootstrap CBs in combination with the subsampling scheme (see Section 6). To

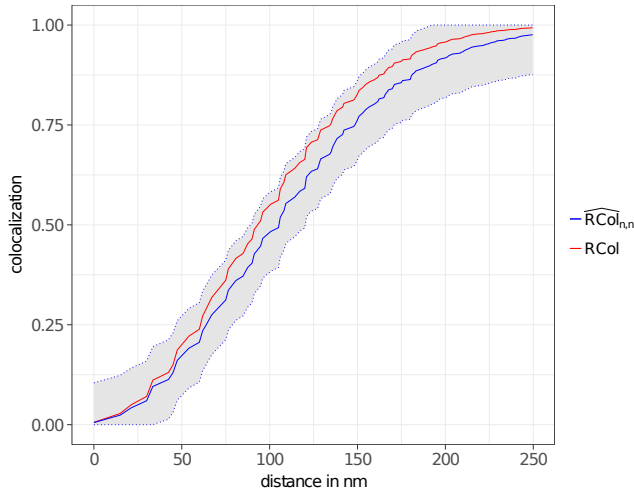


Figure 6: Entropy regularized colocalization for setting two: Staining of ATP Synthase and MIC60 for the zoom in (128×128 image). The sampled regularized colocalization ($\lambda_0 = 0.01$) (solid blue line, subsampling $n = 2000$) with bootstrap confidence bands (gray area between dashed blue lines) based on the n out of n bootstrap with $B = 100$ replications and $\alpha = 0.05$. Red solid line: Population regularized colocalization.

this end, we consider different pairs of zoom ins (128×128 sections) of the STED images in the first column in Figure 5 including the pairs depicted in the middle column. For these instances we are still able to calculate the full regularized colocalization RCol without subsampling. Our goal is to validate that RCol is covered by the bootstrap confidence bands. Statistically speaking after fixing a significance level α , we are interested how close the the empirical coverage probability is to the claimed nominal coverage of $1 - \alpha$. The regularizer f is the entropy (1.4) with amount of regularization given by (5.1) for specified $\lambda_0 > 0$. We subsample $n = 2000$ times according to the intensity distribution of the 128×128 image, calculate $B = 100$ bootstrap replications and set the significance level for the CBs in (7.4) to $\alpha = 0.05$. As an illustrative example, Figure 6 demonstrates a case where RCol is covered by the bootstrap CB.

To gain some intuition how well the empirical coverage probability approximates the nominal coverage probability of $1 - \alpha = 0.95$, we repeat our approach 100 times and report how often RCol is covered by the bootstrap CB. The result is given in Table 2. For bootstrap replications $B = 100$ and rather large amount of regularization $\lambda_0 \in \{0.5, 1, 2\}$ we are close to the nominal coverage probability. For small regularization $\lambda_0 = 0.01$ we obtain

Table 2: Validation of the bootstrap confidence bands. Empirical coverage probability. Subsampling $n = 2000$, bootstrap replications $B = 100$, regularization λ_0 and nominal coverage $1 - \alpha = 0.95$.

Regularization λ_0	Empirical coverage probability
2	0.98
1	0.97
0.5	0.93
0.01	0.88

a slightly smaller empirical coverage probability than desired. This observation is consistent with our empirical analysis for the regularized transport distance in Section 5. There we observed that the approximation by the limit law performs better for larger amount of regularization.

7.1.2 Empirical Colocalization Analysis of the STED Data

Now, we apply our subsampling scheme on the full sized images (666×666 pixels) to evaluate the spatial proximity for each of the two settings, i.e. double staining of *ATPS* (Figure 5 (a)) and staining of *ATPS* and *MIC60* (Figure 5 (b)). We expect the regularized colocalization for setting one (double staining of *ATP Synthase*), say $\text{RCol}^{\text{double}}$, to be large in small distance regimes as most of the transport of pixel intensities should be carried out on small distances. For the regularized colocalization in setting two (staining of *ATP Synthase* and *MIC60*), say $\text{RCol}^{\text{cross}}$, we should observe that there is a significant amount of pixel intensities transported over larger distances resulting in a colocalization that is rather small in the small distance regimes. Recall that in our validation setup we subsampled $n = 2000$ times out of pixel intensities represented by 128×128 images. To achieve comparable accuracy, we require here for 666×666 pixel images a subsampling scheme based on $n = 50.000$ subsamples of the underlying pixel intensity distributions. We then calculate their sampled regularized colocalization, denoted as $\widehat{\text{RCol}}_{n,n}^{\text{double}}$ and $\widehat{\text{RCol}}_{n,n}^{\text{cross}}$, respectively. In order to compare them, we propose to check their difference

$$\widehat{\text{RCol}}_{n,n}^{\text{diff}} := \widehat{\text{RCol}}_{n,n}^{\text{double}} - \widehat{\text{RCol}}_{n,n}^{\text{cross}},$$

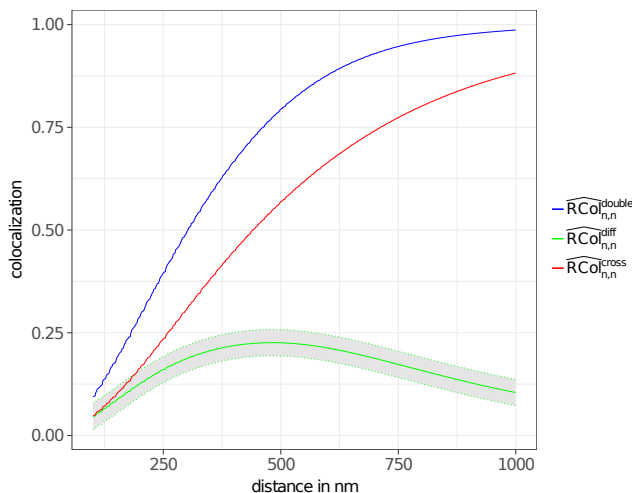


Figure 7: Entropy regularized colocalization analysis. Sampled regularized ($\lambda_0 = 0.01$) colocalization (double staining of ATP Synthase, blue solid line; staining of ATP Synthase and MIC60, red solid line; subsampling $n = 50.000$) based on the images on the left in Figure 5 together with their difference (solid green line) with bootstrap confidence band (gray area between dashed green lines, n out of n bootstrap, $\alpha = 0.05$, $B = 100$ bootstrap replications).

especially in the small distance regime. As before, we obtain CBs by bootstrapping.

The results are presented in Figure 7. We observe that the sampled regularized colocalization $\widehat{\text{RCol}}_{n,n}^{\text{double}}$ (solid blue line) is larger than $\widehat{\text{RCol}}_{n,n}^{\text{cross}}$ (solid red line). Considering their difference $\widehat{\text{RCol}}_{n,n}^{\text{diff}}$ (solid green line) together with the bootstrap CB for the difference (gray area between dashed green lines, $\alpha = 0.05$) demonstrates that the difference is significantly positive at all spatial scales below 1000nm. In fact, our subsampling approach for the regularized colocalization analysis reveals that double staining of *ATP Synthase* is significantly more colocalized than staining of *ATP Synthase* and *MIC60* on all relevant spatial scales as biologically expected.

Acknowledgments

The authors gratefully acknowledge support by the Volkswagen Foundation and the DFG Research Training Group 2088 "Discovering structure in complex data: Statistics meets Optimization and Inverse Problems".

References

- B. K. Abid and R. M. Gower. Greedy stochastic algorithms for entropy-regularized optimal transport problems. *Preprint arXiv:1803.01347*, 2018.
- J. Adler and I. Parmryd. Quantifying colocalization by correlation: The Pearson correlation coefficient is superior to the Mander’s overlap coefficient. *Cytometry A*, 77A(8): 733–742, March 2010. URL <http://doi.wiley.com/10.1002/cyto.a.20896>.
- J. Adler, A. Ringh, O. Öktem, and J. Karlsson. Learning to solve inverse problems using Wasserstein loss. *Preprint arXiv:1710.10898*, 2017.
- J. Altschuler, J. Weed, and P. Rigollet. Near-linear time approximation algorithms for optimal transport via Sinkhorn iteration. In *Advances in Neural Information Processing Systems*, pages 1961–1971, 2017.
- M. Arjovsky, S. Chintala, and L. Bottou. Wasserstein GAN. *Preprint arXiv:1701.07875*, 2017.
- G. Balikas, C. Laclau, I. Redko, and M.-R. Amini. Cross-lingual document retrieval using regularized Wasserstein distance. In *European Conference on Information Retrieval*, pages 398–410. Springer, 2018.
- H. H. Bauschke and P. L. Combettes. *Convex analysis and monotone operator theory in Hilbert spaces*. Springer, 2017.
- J.-D. Benamou, G. Carlier, M. Cuturi, L. Nenna, and G. Peyré. Iterative Bregman projections for regularized transportation problems. *SIAM Journal on Scientific Computing*, 37(2):A1111–A1138, 2015.
- D. P. Bertsekas and D. A. Castanon. The auction algorithm for the transportation problem. *Annals of Operations Research*, 20(1):67–96, 1989.
- J. Bigot, E. Cazelles, and N. Papadakis. Central limit theorems for Sinkhorn divergence between probability distributions on finite spaces and statistical applications. *Preprint arXiv:1711.08947*, 2017.
- P. Billingsley. *Convergence of Probability Measures*. John Wiley & Sons, 2013.
- M. Blondel, V. Seguy, and A. Rolet. Smooth and sparse optimal transport. *Preprint arXiv:1710.06276*, 2017.
- V. Chernozhukov, A. Galichon, M. Hallin, and M. Henry. Monge–Kantorovich depth, quantiles, ranks and signs. *The Annals of Statistics*, 45(1):223–256, 2017.
- J. W. D. Comeau, S. Costantino, and P. W. Wiseman. A guide to accurate fluorescence microscopy colocalization measurements. *Biophysical Journal*, 91(12):4611–4622, 2006.
- M. Cuturi. Sinkhorn distances: Lightspeed computation of optimal transport. In *Advances in Neural Information Processing Systems*, pages 2292–2300, 2013.
- A. Dessein, N. Papadakis, and J.-L. Rouas. Regularized optimal transport and the rot mover’s distance. *Preprint arXiv:1610.06447*, 2016.
- M. Essid and J. Solomon. Quadratically-regularized optimal transport on graphs. *Preprint arXiv:1704.08200*, 2017.
- S. N. Evans and F. A. Matsen. The phylogenetic Kantorovich–Rubinstein metric for environmental sequence samples. *Journal of the Royal Statistical Society: Series B (Statistical Methodology)*, 74(3):569–592, 2012.
- S. Ferradans, N. Papadakis, G. Peyré, and J.-F. Aujol. Regularized discrete optimal transport. *SIAM Journal on Imaging Sciences*, 7(3):1853–1882, 2014.
- A. V. Fiacco. *Introduction to Sensitivity and Stability Analysis in Nonlinear Programming*. Academic Press, Inc., by Springer-Verlag, 1984.
- A. Galichon. *Optimal Transport Methods in Economics*. Princeton University Press, 2016.
- C. Gottschlich and D. Schuhmacher. The shortlist method for fast computation of the

- earth mover’s distance and finding optimal solutions to transportation problems. *PLoS one*, 9(10):e110214, 2014.
- S. W. Hell. Far-field optical nanoscopy. *Science*, 316(5828):1153–1158, 2007.
- L. V. Kantorovich and G. Sh. Rubinstein. On a space of completely additive functions. *Vestnik Leningrad. Univ*, 13(7):52–59, 1958.
- M. Klatt. *Barycenter: Regularized Wasserstein Distances and Barycenters*, 2018. URL <https://CRAN.R-project.org/package=Barycenter>. R package version 1.3.2.
- M. R. Kosorok. *Introduction to Empirical Processes and Semiparametric Inference*. Springer, 2008.
- H. W. Kuhn. The hungarian method for the assignment problem. *Naval Research Logistics (NRL)*, 2(1-2):83–97, 1955.
- H. Ling and K. Okada. An efficient earth mover’s distance algorithm for robust histogram comparison. *IEEE Transactions on Pattern Analysis and Machine Intelligence*, 29(5): 840–853, 2007.
- Y. Lu, L. Chen, and A. Saidi. Optimal transport for deep joint transfer learning. *Preprint arXiv:1709.02995*, 2017.
- David G Luenberger, Yinyu Ye, et al. *Linear and Nonlinear Programming*, volume 2. Springer, 1984.
- G. Luise, A. Rudi, M. Pontil, and C. Ciliberto. Differential properties of Sinkhorn approximation for learning with Wasserstein distance. *arXiv preprint arXiv:1805.11897*, 2018.
- G. Monge. Mémoire sur la théorie des déblais et des remblais. *Histoire de l’Académie Royale des Sciences de Paris*, 1781.
- Victor M Panaretos and Yoav Zemel. Statistical aspects of Wasserstein distances. *Preprint arXiv:1806.05500*, 2018.
- O. Pele and M. Werman. Fast and robust earth mover’s distances. In *IEEE 12th International Conference on Computer Vision*, pages 460–467, 2009.
- G. Peyré, M. Cuturi, et al. Computational optimal transport. Technical report, 2017.
- R Core Team. *R: A Language and Environment for Statistical Computing*. R Foundation for Statistical Computing, Vienna, Austria, 2016. URL <http://www.R-project.org/>.
- S. T. Rachev and L. Rüschendorf. *Mass Transportation Problems: Volume I: Theory*, volume 1. Springer Science & Business Media, 1998.
- R. T. Rockafellar. *Convex Analysis*. Princeton University Press, 1970.
- Y. Rubner, C. Tomasi, and L. J. Guibas. The earth mover’s distance as a metric for image retrieval. *International Journal of Computer Vision*, 40(2):99–121, 2000.
- M. A. Schmitz, M. Heitz, N. Bonneel, F. Ngole, D. Coeurjolly, M. Cuturi, G. Peyré, and J.-L. Starck. Wasserstein dictionary learning: Optimal transport-based unsupervised nonlinear dictionary learning. *SIAM Journal on Imaging Sciences*, 11(1):643–678, 2018.
- B. Schmitzer. A sparse multiscale algorithm for dense optimal transport. *Journal of Mathematical Imaging and Vision*, 56(2):238–259, 2016a.
- B. Schmitzer. Stabilized sparse scaling algorithms for entropy regularized transport problems. *Preprint arXiv:1610.06519*, 2016b.
- J. Schrieber, D. Schuhmacher, and C. Gottschlich. DOTmark—a benchmark for discrete optimal transport. *IEEE Access*, 5:271–282, 2017.
- R. Sinkhorn. A relationship between arbitrary positive matrices and doubly stochastic matrices. *The Annals of Mathematical Statistics*, 35(2):876–879, 1964.
- M. Sommerfeld. *Wasserstein distance on finite spaces: Statistical inference and algorithms*. Dissertation, University of Göttingen, 2017a.
- M. Sommerfeld and A. Munk. Inference for empirical Wasserstein distances on finite

- spaces. *Journal of the Royal Statistical Society: Series B (Statistical Methodology)*, 80 (1):219–238, 2018.
- Max Sommerfeld. *otinference: Inference for Optimal Transport*, 2017b. URL <https://CRAN.R-project.org/package=otinference>. R package version 0.1.0.
- Max Sommerfeld, Jörn Schrieber, and Axel Munk. Optimal transport: Fast probabilistic approximation with exact solvers. *Preprint arXiv:1802.05570*, 2018.
- A. W. van der Vaart. *Asymptotic statistics*, volume 3. Cambridge university press, 2000.
- A. W. van der Vaart and J. A. Wellner. *Weak Convergence*. Springer, 1996.
- C. Villani. *Optimal Transport: Old and New*, volume 338. Springer Science & Business Media, 2008.
- A. G. Wilson. The use of entropy maximising models, in the theory of trip distribution, mode split and route split. *Journal of Transport Economics and Policy*, pages 108–126, 1969.
- L. Xu, D. Rönnlund, P. Aspenström, L. J. Braun, A. K. B. Gad, and J. Widengren. Resolution, target density and labeling effects in colocalization studies - suppression of false positives by nanoscopy and modified algorithms. *FEBS J.*, 283(5):882–898, 2016.
- V. Zinchuk and O. Grossenbacher-Zinchuk. Quantitative colocalization analysis of fluorescence microscopy images. *Current Protocols in Cell Biology*, 62(1):4.19.1–4.19.14, 2014.

A Proofs

A.1 Proof of Theorem 2.3

The first statement that the regularized transport plan $\pi_{\lambda,f}(r_0, s_0)$ in (2.2) is unique and contained in the positive orthant $\mathbb{R}_{>0}^{N^2}$ is well-known, and we refer to [Dessein et al. \(2016\)](#) for further details.

For the second statement we notice that for proper regularizer f the regularized OT (1.3) with marginals r_0 and s_0 fulfills Slater’s constraint qualification ([Bauschke and Combettes, 2017, Proposition 26.18](#)). Hence, strong duality holds and the dual problem admits an optimal solution. Moreover, the regularized transport plan $\pi_{\lambda,f}$ and its corresponding optimal dual solution $\mu_{\lambda,f} \in \mathbb{R}^{2N-1}$ are characterized by the necessary and sufficient Karush-Kuhn-Tucker conditions

$$c + \lambda[\nabla f(\pi_{\lambda,f})]^T - A_{\star}^T \mu_{\lambda,f} = 0, \quad (\text{A.1})$$

$$A_{\star} \pi_{\lambda,f} - [r_0, s_{0\star}]^T = 0. \quad (\text{A.2})$$

The statement of the theorem now follows by an application of the implicit function theorem to the system of equalities (A.1) and (A.2). We define

$$G: \mathbb{R}^{N^2} \times \mathbb{R}^{2N-1} \times \mathbb{R}^{2N-1} \longrightarrow \mathbb{R}^{N^2+2N-1}$$

to be the function given by

$$G(\pi, \mu, (r, s_\star)) = \begin{bmatrix} c + \lambda[\nabla f(\pi)]^T - A_\star^T \mu \\ A_\star \pi - [r, s_\star]^T \end{bmatrix}.$$

The function G is in a neighbourhood of $(\pi_{\lambda,f}, \mu_{\lambda,f}, (r_0, s_{0\star}))$ continuously differentiable with $G(\pi_{\lambda,f}, \mu_{\lambda,f}, (r_0, s_{0\star})) = 0$. The matrix of partial derivatives of G with respect to π and μ is given by

$$\nabla_{(\pi, \mu)} G(\pi_{\lambda,f}, \mu_{\lambda,f}, (r_0, s_{0\star})) = \begin{pmatrix} \lambda \nabla^2 f(\pi_{\lambda,f}) & -A_\star^T \\ A_\star & 0 \end{pmatrix} \in \mathbb{R}^{N^2+2N-1 \times N^2+2N-1}.$$

This matrix is non-singular since $\lambda > 0$, the Hessian $\nabla^2 f(\pi_{\lambda,f})$ is positive by definition of a proper regularizer and the matrix A_\star^T has full rank. The implicit function theorem guarantees the existence of a neighbourhood \mathcal{U} around $(r_0, s_{0\star})$ and a continuously differentiable function $\Theta: \mathcal{U} \rightarrow \mathbb{R}^{N^2} \times \mathbb{R}^{2N-1}$ with components $\Theta(r, s_\star) = (\phi_{\lambda,f}(r, s_\star), \gamma_{\lambda,f}(r, s_\star))$ such that

$$G(\phi_{\lambda,f}(r, s_\star), \gamma_{\lambda,f}(r, s_\star), (r, s_\star)) = 0$$

for all $(r, s_\star) \in \mathcal{U}$. Hence, the vector parametrized by $\phi_{\lambda,f}(r, s_\star)$ fulfills the necessary and sufficient optimality conditions for the regularized OT with feasible set $\mathcal{F}(r, s)$ for $(r, s_\star) \in \mathcal{U}$. In other words, the function $\phi_{\lambda,f}: \mathcal{U} \rightarrow \mathbb{R}^{N^2}$ parametrizes the unique optimal solution for the regularized OT with feasible set $\mathcal{F}(r, s)$ for all $(r, s_\star) \in \mathcal{U}$.

It remains to compute the derivative of $\phi_{\lambda,f}$ at $(r_0, s_{0\star})$. According to the implicit function theorem we obtain that

$$\begin{aligned} \nabla \Theta(r_0, s_{0\star}) &= \begin{bmatrix} \nabla \phi_{\lambda,f}(r_0, s_{0\star}) \\ \nabla \gamma_{\lambda,f}(r_0, s_{0\star}) \end{bmatrix} \\ &= [\nabla_{(\pi, \mu)} G(\pi_{\lambda,f}, \mu_{\lambda,f}, (r_0, s_{0\star}))]^{-1} \begin{bmatrix} 0_{N^2 \times 2N-1} \\ I_{2N-1 \times 2N-1} \end{bmatrix} \\ &= \begin{bmatrix} [\nabla^2 f(\pi_{\lambda,f})]^{-1} A_\star^T [A [\nabla^2 f(\pi_{\lambda,f})]^{-1} A_\star^T]^{-1} \\ -[A_\star [\nabla^2 f(\pi_{\lambda,f})]^{-1} A_\star^T]^{-1} \end{bmatrix}, \end{aligned}$$

where in the second equality the indices denote the size of the zero matrix and identity matrix, respectively, For the last equality we applied a result by [Fiacco \(1984, equalities 4.2.8\)](#).

A.2 Proof of Theorem 3.1

Since the vector $n\hat{r}_n$ follows a multinomial distribution with probability vector r , the multivariate central limit theorem yields

$$\sqrt{n}(\hat{r}_n - r) \xrightarrow{D} \mathcal{N}_N(0, \Sigma(r)).$$

The multivariate delta method in conjunction with the sensitivity analysis for regularized transport plans concludes the statement. More precisely, we obtain that

$$\begin{aligned} \sqrt{n} \{ \pi_{\lambda, f}(\hat{r}_n, s) - \pi_{\lambda, f}(r, s) \} &= \sqrt{n} \{ \phi_{\lambda, f}(\hat{r}_n, s_\star) - \phi_{\lambda, f}(r, s_\star) \} \\ &\xrightarrow{D} \mathcal{N}_{N^2}(0, \nabla_r \phi_{\lambda, f}(r, s_\star) \Sigma(r) [\nabla_r \phi_{\lambda, f}(r, s_\star)]^T). \end{aligned}$$

This finishes the proof.

A.3 Proof of Theorem 3.2

Let $G \sim \mathcal{N}_{N^2}(0, \Sigma_{\lambda, f}(r|s))$ be a N^2 -dimensional Gaussian random vector distributed according to the limit distribution in Theorem 3.1. The multivariate delta method yields

$$\begin{aligned} &\sqrt{n} \{ W_{p, \lambda, f}(\hat{r}_n, s) - W_{p, \lambda, f}(r, s) \} \\ &= \sqrt{n} \left\{ \langle c, \pi_{\lambda, f}(\hat{r}_n, s) \rangle^{\frac{1}{p}} - \langle c, \pi_{\lambda, f}(r, s) \rangle^{\frac{1}{p}} \right\} \xrightarrow{D} \gamma^T G, \end{aligned}$$

where γ is the gradient of the function $\pi \mapsto \langle c, \pi \rangle^{\frac{1}{p}}$ evaluated at the regularized transport plan $\pi_{\lambda, f}(r, s)$. The variance of the real-valued random variable $\gamma^T G$ is given by

$$\sigma_{p, \lambda, f}^2(r|s) = \gamma^T \Sigma_{\lambda, f}(r|s) \gamma.$$

In particular, the variance $\Sigma_{\lambda, f}(r|s)$ is continuous in r . Consequently, by the strong law of large numbers $\hat{r}_n \xrightarrow{a.s.} r$ and the continuous mapping theorem we have that $\sigma_{p, \lambda, f}^2(\hat{r}_n|s) \xrightarrow{a.s.} \sigma_{p, \lambda, f}^2(r|s)$ which together with Slutsky's theorem ([van der Vaart, 2000, Lemma 2.8](#)) concludes the statement.

A.4 Proof of Theorem 7.1

The map $\pi \mapsto R\text{Col}(\pi)$ is linear and Lipschitz with constant at most one. Hence, according to our distributional limit results in Theorem 3.1 for the

regularized optimal transport plan and the continuous mapping theorem ([van der Vaart, 2000, Theorem 18.11](#)) we conclude that

$$\sqrt{n} \left\{ \widehat{RCol}_n - RCol \right\} = RCol(\sqrt{n} \{ \pi_{\lambda, f}(\hat{r}_n, s) - \pi_{\lambda, f}(r, s) \}) \xrightarrow{D} RCol(G),$$

where $G \sim \mathcal{N}_{N^2}(0, \Sigma_{\lambda, f}(r|s))$.